# The electrode/electrolyte reactivity of LiFe0.33Mn 0.67PO4 compared to LiFePO4

Aurélie Guéguen, Laurent Castro, Rémi Dedryvère, E. Dumont, J. Bréger, C. Tessier, Danielle Gonbeau

# The Electrode/Electrolyte Reactivity of $LiFe_{0.33}Mn_{0.67}PO_4$ Compared to $LiFePO_4$

A. Guéguen [a], L. Castro [a], R. Dedryvère [a,*], E. Dumont [b], J. Bréger [b], C. Tessier [b], D. Gonbeau [a]

[a] IPREM-ECP (UMR 5254 CNRS), University of Pau, Hélioparc, 2 av. Pierre Angot 64053 Pau cedex 9, France

[b] SAFT, 111-113 bd. Alfred Daney, 33074 Bordeaux cedex, France

## Abstract

Manganese-rich olivine $LiFe_{0.33}Mn_{0.67}PO_4$ was proven to be an interesting electrode material for Li-ion batteries. In this paper we focus on its electrode/electrolyte reactivity that could play a role in aging processes of $LiFe_{0.33}Mn_{0.67}PO_4$ // graphite cells. Positive and negative electrodes of $LiFe_{0.33}Mn_{0.67}PO_4$ // graphite cells were analyzed by X-Ray Photoelectron Spectroscopy (XPS) at different steps of the first electrochemical cycle to investigate the influence of the working potential increase of this material (as compared to $LiFePO_4$) on the formation of passivation films at the surface of both electrodes. The higher working potential of $LiFe_{0.33}Mn_{0.67}PO_4$ causes an increased reactivity towards the electrolyte with a redox process between $Mn^{3+}$ and carbonates solvents at the outermost surface of the electrode material. It results in a thicker interface layer with respect to $LiFePO_4$. However this interface remains very thin. Some influence on the passivation film formed at the graphite surface was also evidenced.

Keywords: Lithium-ion batteries, phosphate, olivine, manganese, SEI, XPS

* corresponding author (remi.dedryvere@univ-pau.fr)

## 1. Introduction

Li-ion batteries are widely used in portable devices such as cell phones and cameras. Currently further research on Li-ion batteries mainly aims at developing new systems for urban transportation (electric or hybrid vehicles) and electrochemical storage of renewable energies. Several criteria are to take into account when evaluating candidates as positive electrode materials. Energy density, power density, structural stability, and cost are among the most important ones. Phospho-olivine materials $LiMPO_4$ (M=Fe, Mn, Co) have attracted a lot of attention since they were proposed in 1997 by Padhi *et al.*[1, 2] $LiFePO_4$, the most studied phosphate compound for such applications, presents a high theoretical capacity (~170 mAh/g), a rather good working voltage ~3.5 V *vs.* $Li^+/Li^0$, an excellent thermal stability of its delithiated phase $FePO_4$ and a good cycle life. It is also an inexpensive and nontoxic material. Its main drawback, a low intrinsic ionic and electronic conductivity, has been overcome by optimizing its synthesis conditions, *e.g.* by preparing nanoparticles coated with carbon.[3-6] $LiMnPO_4$ could be a more suitable cathode material because of its higher working voltage (4.1 V *vs.* $Li^+/Li^0$), resulting in a higher energy density.[1] However, low capacity and slow kinetics were achieved up to now for this material.[1, 7, 8] Several reasons have been proposed to explain these poor electrochemical performances: lower intrinsic electronic conductivity ($\sigma_e < 10^{-10}$ S/cm for $LiMnPO_4$ and $10^{-9}$ S/cm for $LiFePO_4$ at room temperature),[9, 10] local lattice distortion around Jahn-Teller active $Mn^{3+}$ ions,[11] larger mechanical strains at the boundary between Li-rich and Li-poor phases.[12] Coating $LiMnPO_4$ nanoparticles by conductive carbon helped improving its electrochemical performance, but up to now this material cannot be envisaged as positive electrode for Li-ion batteries.[13-16]

Higher electrochemical rate capability and larger reversible capacity were reported for $LiFe_{1-y}Mn_yPO_4$ compounds as compared to $LiMnPO_4$.[17-19, 7] Yamada et *al.* carried out a detailed study to determine the $Li_xFe_{1-y}Mn_yPO_4$ ($0 \leq x, y \leq 1$) phase diagram.[11] They showed that lithiated $LiFe_{1-y}Mn_yPO_4$ compounds form a solid solution at all relative Fe and Mn concentrations (small difference between the ionic radii of high spin $Fe^{2+}$ and high spin $Mn^{2+}$). On the contrary, for Mn-rich compounds ($y \geq 0.8$) delithiated $Fe_{1-y}Mn_yPO_4$ phases were found to be unstable because of the large anisotropic Jahn-Teller distortion due to $Mn^{3+}$ ions. As a result, Mn-rich $LiFe_{1-y}Mn_yPO_4$ ($y \geq 0.8$) compounds were considered unsuitable for battery applications whereas significantly improved electrochemical performance was observed for $0 \leq y \leq 0.75$. [7, 20]

Recently we have focused on the Mn-rich $LiFe_{0.33}Mn_{0.67}PO_4$ electrode material. In a first paper, we have reported the study of $LiFe_{0.33}Mn_{0.67}PO_4$ // $Li^0$ half-cells by X-Ray Absorption Spectroscopy (XAS), $^{57}Fe$ Mössbauer spectroscopy and X-Ray Photoelectron Spectroscopy (XPS).[21] A reversible capacity of ~150 $mAh.g^{-1}$ at C/20 and 60 °C was observed at the first cycle and a good cyclability was evidenced over 50 cycles at C/6 and 60 °C. The good reversibility of redox processes was confirmed by analysis techniques. Our aim in the present paper is to focus on the electrode/electrolyte interfacial reactivity of this electrode material. Indeed, due to the increase of the working potential of $LiFe_{0.33}Mn_{0.67}PO_4$ with respect to $LiFePO_4$, some increased reactivity towards the electrolyte can be expected. We decided to focus on $LiFe_{0.33}Mn_{0.67}PO_4$ // graphite cells that are closer to the actual conditions of industrial applications and more appropriate for an investigation of possible chemical interactions between both electrodes. Positive and negative electrodes were analyzed by XPS, a suitable surface-sensitive technique to investigate electrode/electrolyte interfaces. The results are compared to reference $LiFePO_4$ // graphite cells in similar experimental conditions.

## 2. Experimental section

### *2-1. Electrochemical details*

The positive electrodes were prepared by coating an aluminium foil current collector with a slurry composed of active material, poly(vinylidene fluoride) PVdF binder and conductive carbon black in *N*-methyl-2-pyrrolidone. The active materials, provided by Süd-Chemie (Moosburg, Germany), were carbon-coated C-$LiFePO_4$ and C-$LiFe_{0.33}Mn_{0.67}PO_4$ prepared by hydrothermal way and will be simply called $LiFePO_4$ and $LiFe_{0.33}Mn_{0.67}PO_4$ for more clarity. The negative electrode consisted of a mixture of round-shape graphite, styrene butadiene rubber (SBR) and carboxymethylcellulose (CMC) sodium salt as binders, deposited on a copper foil current collector. The electrodes were then dried in an oven at 120 °C for 12 hours under vacuum. Coin cells were assembled with 18 mm positive electrodes and 20 mm negative electrodes in an MBraun (Garching, Germany) argon dry box, inside which the oxygen and water contents were maintained below 1 ppm. Separators The separator was a trilayer PP-PE-PP (polyethylene, polypropylene) purchased from Celgard (Charlotte, North Carolina, USA) and the standard liquid electrolyte was a blend of ethylene carbonate (EC), propylene carbonate (PC), and dimethyl carbonate (DMC) with $LiPF_6$ salt and one percent of vinylene carbonate (VC) additive.

Galvanostatic charge/discharge of $LiFePO_4$ // graphite and $LiFe_{0.33}Mn_{0.67}PO_4$ // graphite coin cells was performed using a multichannel potentiostat/galvanostat testing apparatus (Bio-Logic SAS, Claix, France) at 60 °C and with a C/20 rate (*i.e.* the full charge or discharge capacity of the cell is reached within 20 hours). Then, the electrodes were carefully separated from the rest of the battery components in an argon dry box and the electrolyte was removed from the surface

by dilution in DMC before XPS analysis. To ensure a good reproducibility of the results, the same washing procedure was used for all the samples: the electrodes were soaked 3×3 minutes in three successive baths of pure DMC (80 $cm^3$) under mild stirring, then the electrodes were dried 5 min under vacuum.

*2-2. XPS analyses*

The XPS spectrometer was fitted with an argon dry box through a transfer chamber, so that the electrodes could be placed onto the sample holder without any moisture/air exposure or contamination. The analyses were carried out with a Kratos Axis Ultra spectrometer (Kratos Analytical Ltd, Manchester, UK) using a focused monochromatized Al Kα radiation (hν = 1486.6 eV). The spectrometer was calibrated using the photoemission line Ag $3d_{5/2}$ (binding energy 368.3 eV). For the Ag $3d_{5/2}$ line, the full width at half maximum (FWHM) was 0.58 eV under the recording conditions. Core peaks and valence spectra were recorded with a constant 20 eV pass energy. The analyzed area of the samples was 300×700 $\mu m^2$, and the pressure in the analysis chamber was ca. $10^{-7}$ Pa. The binding energy scale was calibrated using the C 1s peak of the hydrocarbon contamination at 285.0 eV. Core peaks were analyzed using a nonlinear Shirley-type background.[22] The peak positions and areas were optimized by a weighted least-square fitting method using 70% Gaussian, 30% Lorentzian lineshapes. Quantification was performed on the basis of Scofield's relative sensitivity factors.[23]

## 3. Results and discussion

*3.1. Electrochemical cycling*

Figure 1 shows a comparison of the first electrochemical cycles of $LiFePO_4$ (2.5-3.7 V) and

$LiFe_{0.33}Mn_{0.67}PO_4$ (2.5-4.3 V) obtained at 60 °C in coin cells *vs.* Li and *vs.* graphite negative electrodes. Corresponding values of first charge capacity and irreversible discharge capacity are reported in Table 1. The $LiFePO_4$ // $Li^0$ cell presents a first charge capacity of 152 $mAh.g^{-1}$ and no irreversible capacity. The discharge capacity is even slightly higher (4 $mAh.g^{-1}$) than the charge capacity due to the reduction upon discharge of the $Fe^{3+}$ impurities that are present in the starting $LiFePO_4$ material, especially at the surface.[24-27]

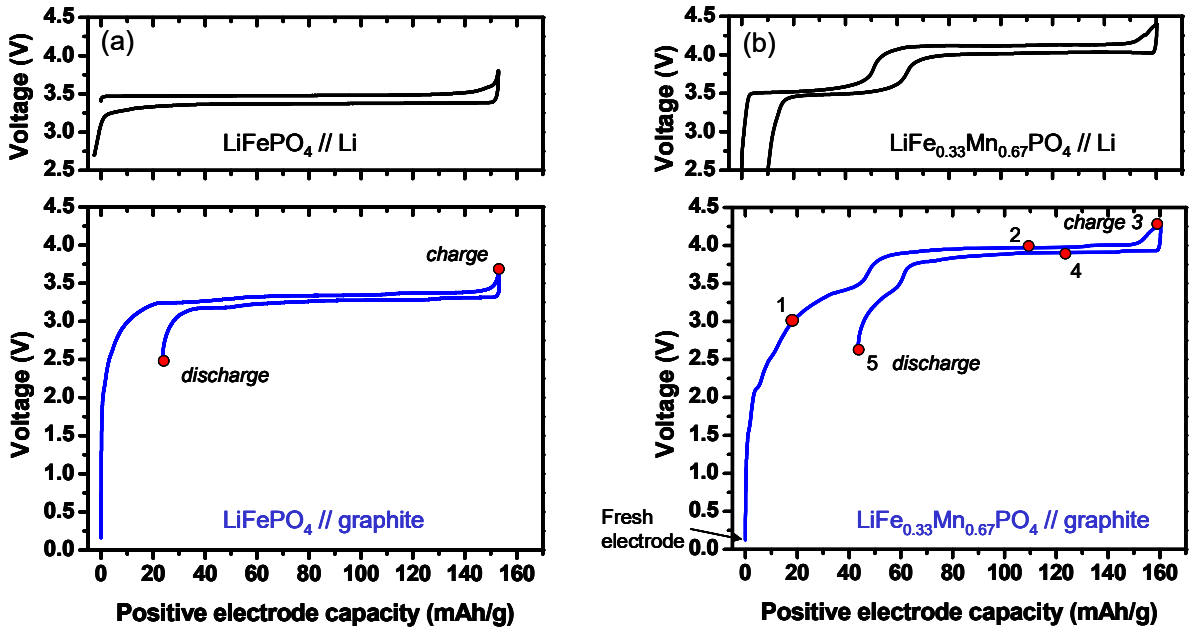


**Figure 1**. First electrochemical cycle obtained in coin cells at 60 °C and C/20 rate for (a) $LiFePO_4$ and (b) $LiFe_{0.33}Mn_{0.67}PO_4$ positive electrodes *vs.* Li and graphite. Points 1-5 refer to $LiFe_{0.33}Mn_{0.67}PO_4$ // graphite cells analyzed by XPS.

The $LiFePO_4$ // graphite cell presents a first charge capacity of 153 $mA.g^{-1}$ and an irreversible capacity of 24 mAh/g. This latter is mainly due to the loss of lithium ensuing from the formation of the Solid Electrolyte Interphase (SEI) at the surface of the graphite negative electrode.[24, 28]

**Table 1.** Positive electrode capacities measured for the different cells presented in Figure 1.

| | $LiFePO_4$ | | $LiFe_{0.33}Mn_{0.67}PO_4$ | |
|---|---|---|---|---|
| | *vs.* $Li^0$ | *vs.* graphite | *vs.* $Li^0$ | *vs.* graphite |
| First charge capacity (mAh/g) | 152 | 153 | 160 | 160 |
| Irreversible first discharge capacity (mAh/g) | 0 | 24 | 10 | 44 |

The $LiFe_{0.33}Mn_{0.67}PO_4$ // $Li^0$ cell exhibits two distinct plateaus upon charge and discharge: the first one at ~3.5 V corresponds to iron oxidation/reduction, the second one at ~4.1 V corresponds to manganese. The lengths of Fe and Mn plateaus are roughly proportional to the Fe/Mn ratio in the nominal composition of the active material.

The $LiFe_{0.33}Mn_{0.67}PO_4$ // $Li^0$ cell shows a first charge capacity of 160 $mA.g^{-1}$ and an irreversible capacity of 10 mAh/g that was not observed for $LiFePO_4$ // $Li^0$. This point will be discussed later. The $LiFe_{0.33}Mn_{0.67}PO_4$ // graphite cell exhibits the same first charge capacity as that obtained *vs.* $Li^0$. In this case the Fe charge plateau is less clearly observed during charge (point 1) as the electrochemical curve of the full cell results from both cathode and anode contributions. Thus the voltage increase observed between 0 and 30 mAh/g is mainly assigned to the potential decrease of the graphite electrode at the beginning of charge. Upon discharge, the irreversible capacity is 44 mAh/g, which is significantly higher than for the $LiFePO_4$ // graphite cell. As a result, the Fe discharge plateau is dramatically shortened (point 5) because the remaining amount of lithium that can be reinserted into the positive electrode active material is not sufficient. Indeed, since some part of the active lithium has been lost upon charge, there is not enough lithium in the graphite negative electrode to fully re-insert into the positive electrode upon discharge. As a result, the cell voltage drops before the expected discharge capacity value

(*i.e.* the voltage decrease of point 5 is assigned to a potential increase of the graphite electrode and not to a potential decrease of the $LiFe_{0.33}Mn_{0.67}PO_4$ electrode).

As a summary, whether a metallic lithium or a graphite electrode is used, a higher irreversible capacity is observed when using a $LiFe_{0.33}Mn_{0.67}PO_4$ positive electrode as compared to $LiFePO_4$. In both cases an irreversible capacity is observed when using a graphite electrode, following the formation of the SEI, but a greater irreversible capacity is observed for $LiFe_{0.33}Mn_{0.67}PO_4$. Several hypotheses can be given: *(i)* A small part of the observed charge capacity is due to oxidation of the electrolyte instead of oxidation of Mn and lithium extraction from the positive electrode active material, *(ii)* A part of the active lithium cannot be reinserted into the $LiFe_{0.33}Mn_{0.67}PO_4$ olivine structure upon discharge due to phase transitions, or because a small part of the active material has been damaged (by dissolution in the electrolyte for example). However, previous works have shown that a good capacity retention upon cycling (over more than 50 cycles) is observed when using a metallic lithium electrode, which is a continuous source of active lithium.[21] This shows that the irreversible capacity is not due to damages of the $LiFe_{0.33}Mn_{0.67}PO_4$ active material, and that the loss of active lithium can be overcome by lithium replenishment. This suggests that the greater irreversible capacities observed for $LiFe_{0.33}Mn_{0.67}PO_4$ as compared to $LiFePO_4$ are related to the higher working potential of this positive electrode material. The analysis of XPS spectra of positive and negative electrodes will help in grasping more insight into these phenomena.

### *3.2. XPS results*

#### *3.2.1. Study of the Fe and Mn redox processes*

Fe 2p and Mn 2p XPS spectra of the positive electrode recovered at different steps of the first electrochemical cycle of a $LiFe_{0.33}Mn_{0.67}PO_4$ // graphite cell are presented in Figure 2. Mn 2p and Fe 2p spectra consist of two components, namely $2p_{3/2}$ and $2p_{1/2}$ due to spin orbit coupling with an intensity ratio ~2/1. Each component consists of a main peak and a shake-up satellite at about +5 eV binding energy [29].

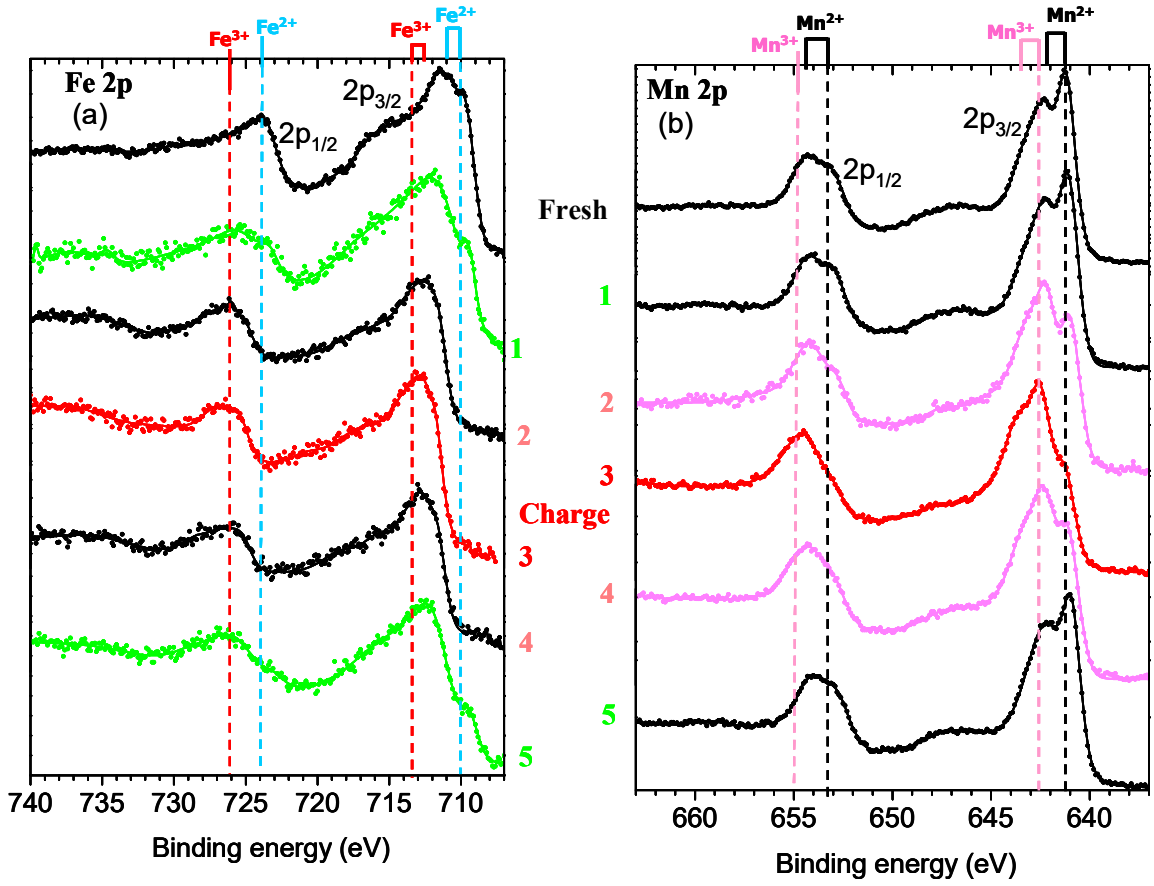


**Figure 2**. (a) Fe 2p and (b) Mn 2p XPS spectra of the $LiFe_{0.33}Mn_{0.67}PO_4$ positive electrode recovered at different steps of the first cycle of the $LiFe_{0.33}Mn_{0.67}PO_4$ // graphite cell.

*Fresh electrode*

The Fe 2p spectrum of the fresh $LiFe_{0.33}Mn_{0.67}PO_4$ electrode shows a main Fe $2p_{3/2}$ peak at 711 eV. The asymmetric shape of the maximum indicates the presence of $Fe^{3+}$ surface impurities accompanying $Fe^{2+}$ cations of the olivine structure.[24, 30] Such $Fe^{3+}$ impurities were also observed for the as-prepared material and do not result from the electrode preparation. It may be due to the formation of $Fe_2O_3$ surface oxide following air exposure at moderate temperature at the end of synthesis process, as suggested by Hamelet *et al.* for $LiFePO_4$-based nanopowders.[25]

The Mn 2p spectrum of the fresh $LiFe_{0.33}Mn_{0.67}PO_4$ electrode shows a complex shape. Mn $2p_{3/2}$ and $2p_{1/2}$ main peaks consist of two fine structures (641 and 642 eV for $2p_{3/2}$). These fine structures do not result from the presence of two different oxidation states of manganese, but from final state effects due to the XPS photoemission process (multiplet splitting effects, or local *vs.* non-local screening effects [31, 32]). This complex shape and the shake-up satellite at +5 eV are characteristic of $Mn^{2+}$ cations in $LiFe_{0.33}Mn_{0.67}PO_4$.[21]

*Point 1 (3.0 V)*

On the first charge "plateau" (point 1), the intensity of the Fe $2p_{3/2}$ peak at 710 eV ($Fe^{2+}$) decreases while a new peak at 712.5 eV appears. This new peak is attributed to $Fe^{3+}$ cations in the delithiated phase.[24, 21] The same evolution can be also clearly observed for the Fe $2p_{1/2}$ component, with the peak at 724 eV ($Fe^{2+}$) partially replaced by a new peak at 726 eV ($Fe^{3+}$). At this stage it is possible to estimate the $Fe^{3+}/Fe^{2+}$ ratio at the surface of the material by fitting the spectrum with a linear combination of the Fe 2p spectra of $FePO_4$ and $LiFePO_4$ reference samples (*i.e.* obtained from the complete charge and discharge of a $LiFePO_4$ // $Li^0$ cell, respectively).[24] At point 1 the $Fe^{3+}/Fe^{2+}$ ratio is ~75/25. No change was noticed in the Mn 2p spectrum at this stage.

*Points 2 and 3: Second charge plateau (4.1 V) and end of charge (4.3 V)*

On the second charge plateau (point 2), the Fe $2p_{3/2}$ component at 710 eV ($Fe^{2+}$) has completely disappeared, only the component at 712.5 eV ($Fe^{3+}$) is still present. Thus all $Fe^{2+}$ ions have been oxidized into $Fe^{3+}$ at this stage. At the end of charge (point 3), no change in the Fe 2p spectrum is observed as all $Fe^{2+}$ have been already oxidized into $Fe^{3+}$.

Concerning manganese, the analysis of Mn 2p spectra shows the partial oxidation of $Mn^{2+}$ into $Mn^{3+}$. The main Mn $2p_{3/2}$ peak (maximum at 641 eV, *i.e.* $Mn^{2+}$) decreases while a new peak at 642.5 eV ($Mn^{3+}$) is gaining intensity. This evolution is confirmed by the Mn $2p_{1/2}$ component, with the $Mn^{2+}$ peak (maximum at 654 eV) being partially replaced by a new $Mn^{3+}$ peak (maximum at 655 eV). At the end of charge a shoulder at 641 eV indicates that all $Mn^{2+}$ cations were not totally oxidized into $Mn^{3+}$. By subtracting the Mn 2p spectrum of the starting $LiFe_{0.33}Mn_{0.67}PO_4$ electrode ($Mn^{2+}$) from the spectra recorded after cycling, it is possible to obtain the Mn 2p spectrum of the theoretically totally delithiated $Fe_{0.33}Mn_{0.67}PO_4$ electrode ($Mn^{3+}$). Then, by fitting the spectra with a linear combination of these $Mn^{2+}$ and $Mn^{3+}$ spectra, it is possible to estimate the $Mn^{3+}/Mn^{2+}$ ratio at the surface of the material upon cycling. At point 2, the $Mn^{3+}/Mn^{2+}$ ratio is ~40/60. At the end of charge it is ~58/42.

*Point 4: First discharge plateau (3.9 V)*

On the Mn discharge plateau (point 4), reverse reduction of $Mn^{3+}$ cations takes place as the Mn $2p_{3/2}$ peak at 641 eV characteristic of $Mn^{2+}$ increases again. The Mn 2p spectrum is rather close to that obtained at point 2, and at this stage the $Mn^{3+}/Mn^{2+}$ ratio is ~36/64. No reduction of $Fe^{3+}$ cations is observed in Fe 2p spectra.

*Point 5: End of discharge (2.5 V)*

At the end of the cycle (point 5), all Mn species at the surface of the $LiFe_{0.33}Mn_{0.67}PO_4$ electrode are in +II oxidation state; which indicates a good reversibility of the redox reaction of the $Mn^{3+}/Mn^{2+}$ couple. Concerning iron, a significant amount of $Fe^{3+}$ cations still remains at the end of discharge, since the $Fe^{3+}/Fe^{2+}$ ratio is ~53/47. This is in good agreement with the very short Fe discharge plateau observed in Figure 1 and the loss of electrochemically active lithium that cannot be reinserted in the $LiFe_{0.33}Mn_{0.67}PO_4$ electrode upon discharge, as discussed above.

As a summary, the different $Fe^{3+}/Fe^{2+}$ and $Mn^{3+}/Mn^{2+}$ ratios determined at the surface of the $LiFe_{0.33}Mn_{0.67}PO_4$ electrode are reported in Table 2.

**Table 2**. $Fe^{2+}/Fe^{3+}$ and $Mn^{2+}/Mn^{3+}$ ratios measured by XPS at the surface of the $LiFe_{0.33}Mn_{0,67}PO_4$ electrode along the first cycle vs. graphite (points 1-5 refer to Fig 1).

| **Point** | $LiFe_{0.33}Mn_{0.67}PO_4$ // graphite | | | |
|---|---|---|---|---|
| | **$Fe^{2+}$** | **$Fe^{3+}$** | **$Mn^{2+}$** | **$Mn^{3+}$** |
| **1** | 75 | 25 | 100 | 0 |
| **2** | 0 | 100 | 60 | 40 |
| **3 (charge)** | 0 | 100 | 42 | 58 |
| **4** | 0 | 100 | 64 | 36 |
| **5 (discharge)** | 47 | 53 | 100 | 0 |

A very interesting feature is the great amount of $Mn^{2+}$ (42%) remaining at the end of charge (point 3). This can be further exploited to understand the behaviour of this electrode. Electrochemical data of $LiFe_{0.33}Mn_{0.67}PO_4$ // graphite cell show that a 100 $mAh.g^{-1}$ reversible plateau at 3.9 V is observed for manganese upon discharge. The theoretical capacity of $LiFe_{0.33}Mn_{0.67}PO_4$ is 170.5 $mAh.g^{-1}$. Taking into account the stoichiometry of the material,

manganese contributes by 113.7 mAh.g$^{-1}$ to this theoretical capacity. This means that a 100 mAh.g$^{-1}$ plateau correspond to 88% of $Mn^{3+}$ ions being reduced into $Mn^{2+}$ upon discharge. Therefore at least 88% of $Mn^{2+}$ ions are oxidized into $Mn^{3+}$ upon charge; however surface analysis by XPS shows that only 58% of $Mn^{3+}$ are present at the surface of the electrode material at the end of charge. Note that this phenomenon is not observed for iron in $LiFePO_4$ // graphite cells (100 % of $Fe^{2+}$ are observed at the end of charge). Our explanation of this phenomenon is that the increase of the working potential of the electrode due to the manganese plateau at 4.1 V results in an enhanced reactivity of the surface of the electrode towards the electrolyte, with a slight oxidation process of the electrolyte accompanied by a partial reduction of $Mn^{3+}$ into $Mn^{2+}$. Note that this phenomenon was already observed in a previous work with $LiMn_{1.6}Ni_{0.4}O_4$ spinel electrodes working at higher potential (nickel plateau at ~4.7 V).[33] Indeed, some part of the nickel was not oxidized at the end of charge up to 5 V. However the present results show that this phenomenon can occur with a 4.1V manganese plateau. A detailed analysis of other XPS spectra will provide additional information on the electrode/electrolyte interfaces on both $LiFe_{0.33}Mn_{0.67}PO_4$ and graphite electrodes.

*3.2.2. Electrode/electrolyte interfaces*

*3.2.2.1 $LiFe_{0.33}Mn_{0.67}PO_4$ positive electrode*

Figure 3 shows O 1s and P 2p spectra of the $LiFe_{0.33}Mn_{0.67}PO_4$ electrode at the different studied points (1-5) upon the first cycle. Results obtained after charge and discharge of a $LiFePO_4$ // graphite cell are also presented for comparison.

*O 1s core peaks:* The O 1s spectrum of the fresh $LiFe_{0.33}Mn_{0.67}PO_4$ electrode consists of a main peak at 531.4 eV, which is the signature of the $(PO_4)^{3-}$ group (Figure 3b).[30]

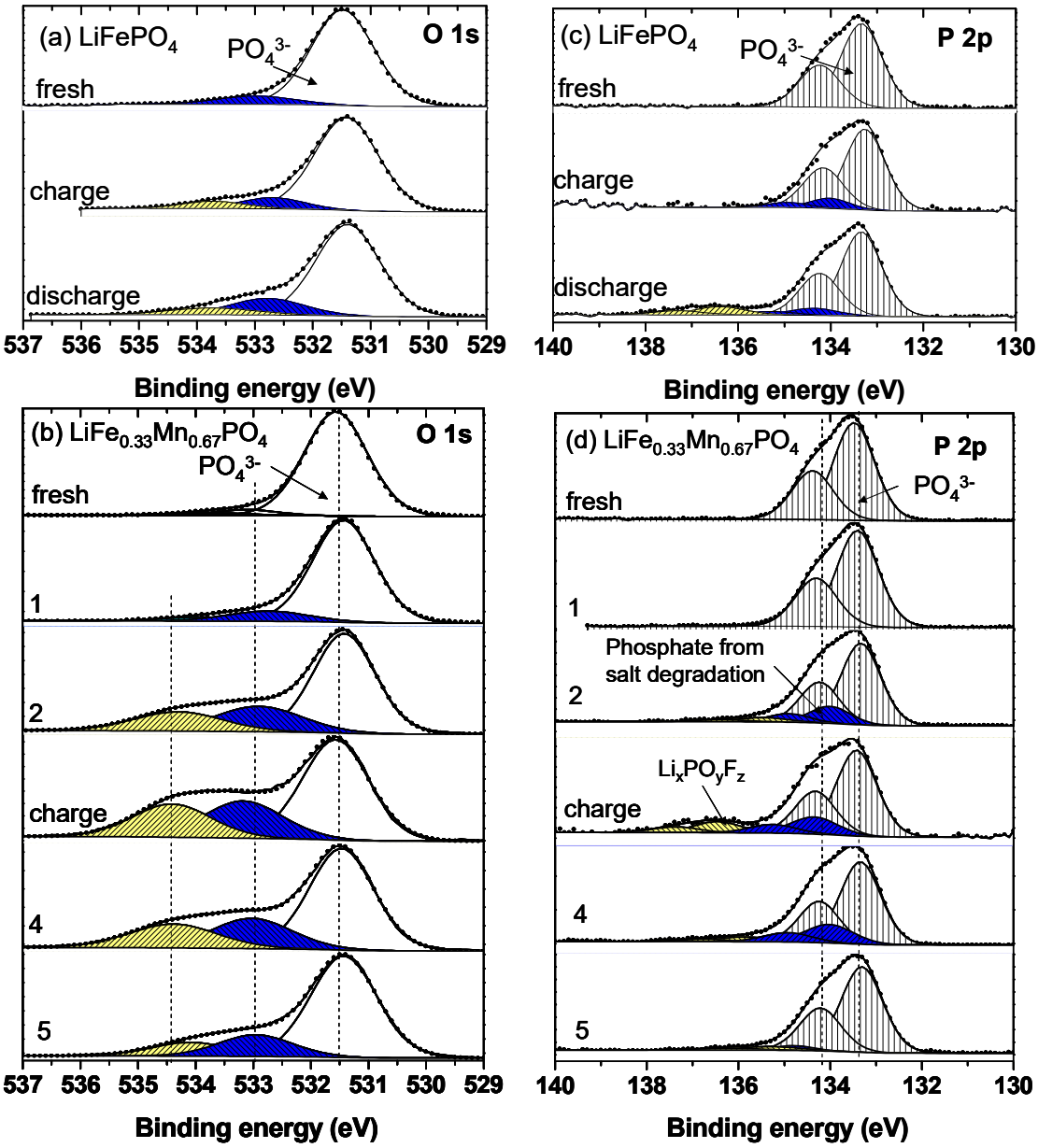


**Figure 3**. (a) O 1s and (c) P 2p XPS spectra of $LiFePO_4$ electrodes recovered at the end of charge and discharge vs. graphite; (b) O 1s and (d) P 2p XPS spectra $LiFe_{0.33}Mn_{0.67}PO_4$ positive electrodes recovered at different steps of the first electrochemical cycle of $LiFe_{0.33}Mn_{0.67}PO_4$ // graphite cells.

The other weak peak at 533 eV is attributed to a weak surface contamination. At the first charge plateau (point 1), slight changes are observed as the peak at 533 eV has gained more intensity and a new peak at 534.5 eV has appeared. These two peaks increase significantly on the Mn charge plateau (point 2) and at the end of charge (point 3) and can be assigned to the deposition of oxygenated species in a passivation film that is formed at the surface of the $LiFe_{0.33}Mn_{0.67}PO_4$ electrode upon charge. Taking into account the depth of analysis of XPS (~5 nm), the film thickness is lower than a few nanometers since the O 1s peak of the active material still remains the main peak of the spectrum, even at the end of charge. However, comparison with a $LiFePO_4$ // graphite cell (Figure 3a) shows that the passivation film formed at the surface of the $LiFePO_4$ electrode upon charge is much thinner. This difference can be attributed to the increase of the working potential of the electrode leading to a higher oxidation of the electrolyte. Upon discharge (points 4 and 5), a decrease of the intensity of the two additional peaks of $LiFe_{0.33}Mn_{0.67}PO_4$ is observed (Figure 3b). This can be interpreted by a partial dissolution of the deposited oxygen-containing species upon discharge.

*P 2p core peaks.* Only one asymmetric $2p_{3/2}$-$2p_{1/2}$ doublet (with $2p_{3/2}$ at 133.4 eV) is present in the P 2p spectrum of the fresh $LiFe_{0.33}Mn_{0.67}PO_4$ electrode (Figure 3d). This binding energy value is characteristic of $(PO_4)^{3-}$ groups in the olivine structure.[30] No surface phosphorus-containing impurity is observed on the fresh electrode surface. At the first charge plateau (point 1), no changes are detected in the P 2p spectrum as compared to the fresh electrode. From the Mn charge plateau (point 2) to the end of the cycle (point 5) a new doublet (with $2p_{3/2}$ at 134 eV) appears, which is attributed to phosphates species resulting from the degradation of $LiPF_6$ salt of the electrolyte. Another P 2p doublet (with $2p_{3/2}$ at 136.4 eV) can be also noticed, especially at the end of charge (point 3), which can be assigned to fluorophosphates $Li_xPO_yF_z$, *i.e.*

intermediate decomposition products of $LiPF_6$. Although these salt degradation products are deposited in a greater amount than at the surface of the $LiFePO_4$ electrode, especially at the end of charge (Figure 3c), the proportion of phosphates and fluorophosphates remains very small as compared to the characteristic P 2p peak of the active material, which shows that these degradation compounds of $LiPF_6$ are not the main source of oxygen detected in the surface film covering the $LiFe_{0.33}Mn_{0.67}PO_4$ electrode. It is thus expected that the main source of oxygen are degradation compounds of the solvents (EC, PC and DMC). Therefore the analysis of C 1s spectra of these samples should be very fruitful.

*C 1s core peaks.* Figure 4a shows the C 1s spectra of the fresh $LiFe_{0.33}Mn_{0.67}PO_4$ electrode (white) and after full charge at 4.3 V (point 3, grey). Comparison with a $LiFePO_4$ // graphite cell in the same conditions is given in Figure 4b. The C 1s spectrum of the fresh $LiFe_{0.33}Mn_{0.67}PO_4$ and $LiFePO_4$ positive electrodes are dominated by the peaks of the carbon-containing additives (carbon black at 285 eV and PVdF binder at 286.5 and 290.9 eV). Due to the great surface area of carbon black nanoparticles and to the binding behavior of PVdF, the total amount of these additives as measured by XPS at the surface of the electrode is about 60 %, *i.e.* much greater than their actual proportion in the electrode. For this reason, it is possible to detect the presence of other carbonaceous species only if they are deposited in a great amount at the surface, and few differences could be noticed in the C 1s spectra upon the first cycle. Only the C 1s spectrum of the $LiFe_{0.33}Mn_{0.67}PO_4$ electrode obtained at the end of charge at 4.3 V (grey in Figure 4a) was sufficiently different from the starting electrode to bring some information, by subtracting the spectrum of the fresh $LiFe_{0.33}Mn_{0.67}PO_4$ electrode (white) in order to evidence the differences. The fitting of this subtracted spectrum displays the appearance of several components corresponding to $CH_2$, C-O, C=O and O=C–O environments of carbon, corresponding to an

amount of carbon ~ 13 % of the total signal of elements at the surface of the electrode. Taking into account the nature of the various environments of carbon, the total amount of carbon and oxygen attributed to organic species ensuing from degradation of the solvents and deposited at the surface of the electrode is 26 %. However, it is not possible from these data to exactly identify the species. We can just notice that the deposition of carbonates is not evidenced in this case because the characteristic peak of carbonates at 290 eV is not observed. Comparison with the $LiFePO_4$ // graphite cell by doing the same kind of analysis (Figure 4b) evidences the much lower amount of organic oxygenated species deposited at the surface of the $LiFePO_4$ electrode.

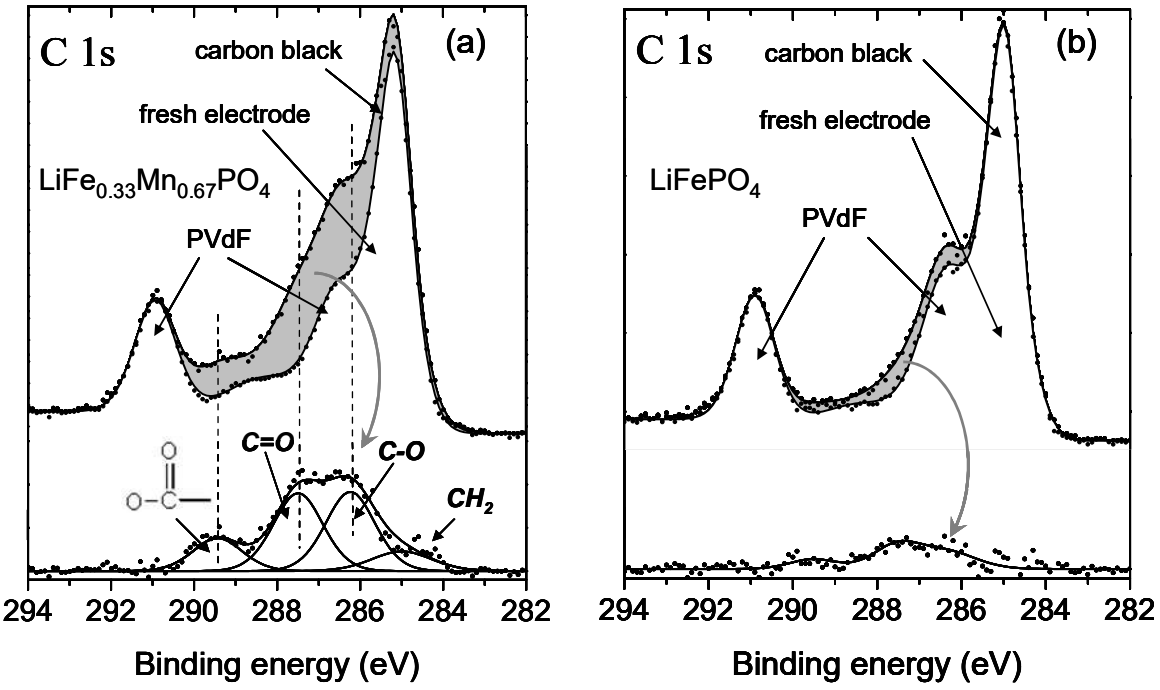


**Figure 4**. C 1s XPS spectra of (a) the $LiFe_{0.33}Mn_{0.67}PO_4$ and (b) the $LiFePO_4$ positive electrodes recovered at the end of charge versus graphite; both the C 1s spectra of the electrode at end of charge (grey) and of the fresh electrode (white) are represented. The difference between both spectra is represented in the bottom part.

The signal to noise ratio of the subtracted spectrum is too bad in this case to extract precise information about the nature of carbon environments in the surface film, but no significant differences with respect to $LiFe_{0.33}Mn_{0.67}PO_4$ are displayed at this stage.

As a summary, comparison between $LiFe_{0.33}Mn_{0.67}PO_4$ and $LiFePO_4$ shows that XPS spectra do not significantly differ by the nature of the deposited species observed at the surface, but significantly differ by the amounts of deposited species. The amount of deposited species is much higher in the case of $LiFe_{0.33}Mn_{0.67}PO_4$.

These observations are in good agreement with the conclusion that the enhanced reactivity of the $LiFe_{0.33}Mn_{0.67}PO_4$ electrode surface towards the electrolyte results from the increase of the potential of the charge/discharge plateau (Mn plateau at 4.1 V) as compared to $LiFePO_4$. According to XPS analyses the surface chemistry of the $LiFe_{0.33}Mn_{0.67}PO_4$ electrode after charge up to point 1 (first Fe charge "plateau") is similar to the surface chemistry of the $LiFePO_4$ electrode after a full charge. A more significant amount of deposited species is found at the $LiFe_{0.33}Mn_{0.67}PO_4$ surface after charge over the Mn charge plateau (4.1 V). Additional carbonaceous species are clearly observed in the C 1s spectrum of the $LiFe_{0.33}Mn_{0.67}PO_4$ electrode at the end of charge. The presence of different mono- and di-oxygenated environments of carbon at the surface of the electrode indicates an oxidation of the electrolyte solvents. Such side reactions between the electrode surface and the electrolyte result in the reduction of $Mn^{3+}$ from the extreme surface of the electrode into $Mn^{2+}$. This explains the lower amount of $Mn^{3+}$ observed by XPS at the end of charge at the extreme surface of the $LiFe_{0.33}Mn_{0.67}PO_4$ electrode as compared to the expected amount in the bulk electrode from electrochemical data.

*3.2.2.2 Graphite negative electrode*

C 1s spectra of the graphite electrode recovered after charge (point 3) and discharge (point 5) of the $LiFe_{0.33}Mn_{0.67}PO_4$ // graphite cell are presented Figure 5a. The C 1s spectrum of the fresh electrode consists of a main peak at 284 eV assigned to graphite, a second component at 285 eV corresponding to $CH_2$ environment in the polymeric binder SBR, and two minor peaks at 286.4 and 288.2 eV attributed to CO and COO environments of carbon in CMC binder, respectively.

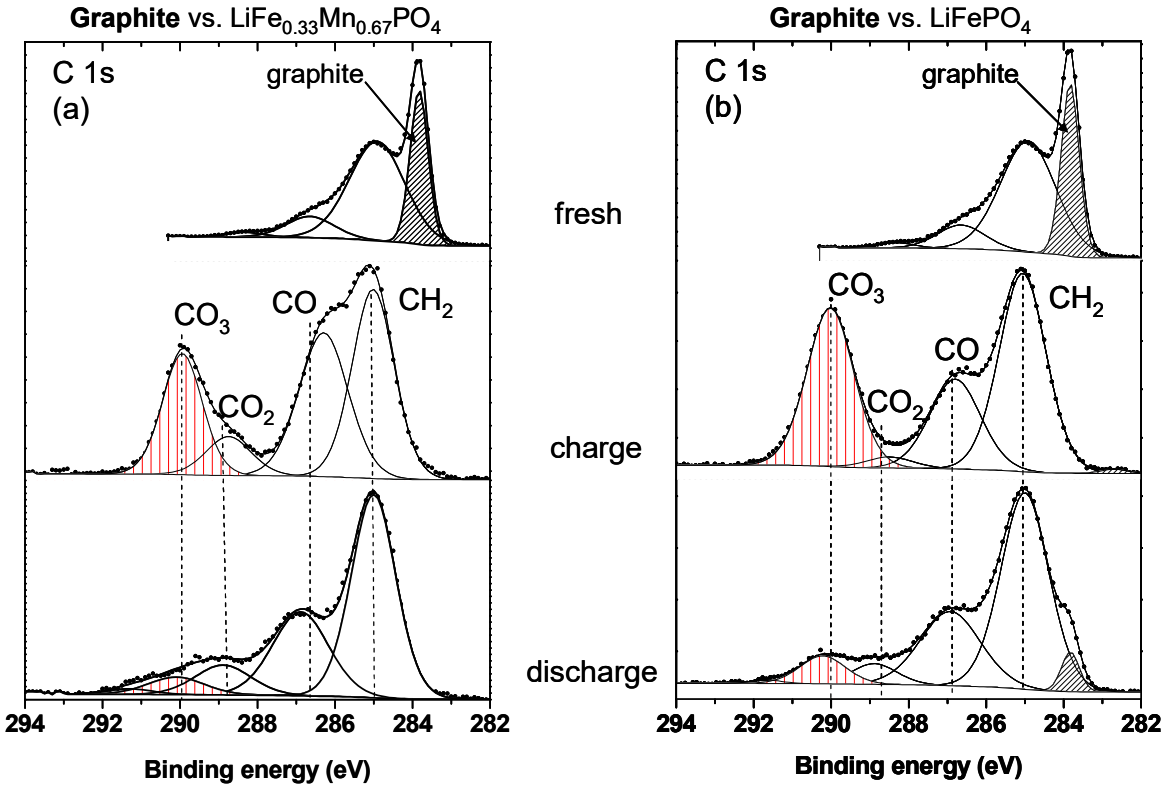


**Figure 5**. C 1s XPS spectra of the negative graphite electrode recovered after charge and discharge during the first cycle vs. (a) $LiFe_{0.33}Mn_{0.67}PO_4$ and (b) $LiFePO_4$.

At the end of charge of the $LiFe_{0.33}Mn_{0.67}PO_4$ // graphite cell (Figure 5a), the graphite component is no longer visible, which means the electrode is fully covered by a passivation layer thicker than 5 nm. At the end of discharge, the graphite is still hidden by the species deposited at

its surface. Four new components are observed in the C 1s spectra with binding energies of about 285, 287, 289 and 290 eV, attributed to $CH_2$, CO, $CO_2$ and $CO_3$ environments, respectively. Note that these XPS C 1s signatures are commonly observed at the surface of graphite electrode after cycling of a usual $LiCoO_2$ // graphite cell.[34] At this stage, no significant change can be noticed relative to the chemical nature of the positive electrode. Such deposited species result from the decomposition of the solvents to form the Solid Electrolyte Interphase (SEI), and several mechanisms have been proposed in the literature to explain its formation. The $CO_3$ component can be explained by the formation of $Li_2CO_3$ or lithium alkyl carbonates ($ROCO_2Li$) ensuing from the reduction of carbonate solvents.[35, 36] The C-O component may be assigned to lithium alkyl carbonates ($\underline{C}H_3OCO_2Li$ for example) and/or to $(-CH_2-CH_2-O-)_n$ oligomers.[37] The $CO_2$ component may be attributed to the formation of oxalates.[38] In Figure 5a we can observe a significant decrease of the $CO_3$ and CO components upon discharge. Such an effect was also previously observed with $LiCoO_2$ // graphite cells.[34] It could be interpreted by a partial redissolution of carbonates species upon discharge, which means that a minor part of the SEI can be dissolved upon discharge although the formation of the SEI is mainly an irreversible process.

Comparison with a $LiFePO_4$ // graphite cell in the same conditions is given in Figure 5b. At the end of charge, the lithiated graphite component is hardly detectable (weak peak at 283 eV) but it has not totally disappeared and thus the SEI is slightly thinner than after cycling *vs.* $LiFe_{0.33}Mn_{0.67}PO_4$. At the end of discharge a small graphite peak is again visible by a shoulder at 283.5 eV, showing a slight decrease of the SEI thickness. The same phenomenon of redissolution of carbonates species upon discharge is observed.

As a summary, even if the nature of the positive electrode ($LiFe_{0.33}Mn_{0.67}PO_4$ or $LiFePO_4$) has a weak influence on the graphite electrode/electrolyte interface, a slightly thicker SEI is observed

*vs.* $LiFe_{0.33}Mn_{0.67}PO_4$, showing that the electrode/electrolyte reactivity at the positive electrode side has some influence at the negative electrode side. Moreover, a small amount of manganese originating from the $LiFe_{0.33}Mn_{0.67}PO_4$ positive electrode was also detected on the graphite negative electrode (~ 0.5 at.%) at the end of charge and discharge. This result is confirmed by X-ray fluorescence (XRF) experiments showing that the Fe and Mn contents in the graphite electrode after charge are 100 and 200 ppm, respectively (note that these values are much lower than XPS because XPS analysis strictly concerns the surface of the electrode, where the metals are deposited). As a result the communication between both electrodes is actually evidenced. Some other species formed by oxidation of the electrolyte components at the surface of the higher voltage $LiFe_{0.33}Mn_{0.67}PO_4$ electrode may be also transferred to the graphite electrode and modify its surface chemistry. This phenomenon was already evidenced for high voltage spinel positive electrodes [33]. A slight difference between the behaviours of $LiFePO_4$ and $LiFe_xMn_{1-x}PO_4$ is expected due to the voltage difference between both materials. The same way, some species formed by reduction at the surface of the negative electrode can be transferred to the positive electrode.

## 4. Conclusion

The positive and negative electrodes of a $LiFe_{0.33}Mn_{0.67}PO_4$ // graphite cell were analyzed using XPS technique after charge and discharge at different steps of the first electrochemical cycle. Study of Fe 2p and Mn 2p XPS core peaks showed a good reversibility of the redox processes. The higher working potential of $LiFe_{0.33}Mn_{0.67}PO_4$ with respect to $LiFePO_4$ results in an increased reactivity of the $LiFe_{0.33}Mn_{0.67}PO_4$ electrode surface towards the electrolyte. In both cases ($LiFe_{0.33}Mn_{0.67}PO_4$ and $LiFePO_4$) a part of the electrochemically active lithium is

consumed for the SEI formation on the graphite electrode. In the case of the $LiFe_{0.33}Mn_{0.67}PO_4$ electrode, a thicker passivation film is also observed on the positive electrode surface, resulting from the oxidation of the electrolyte solvents. This enhanced electrode/electrolyte reactivity causes the reduction of part of the $Mn^{3+}$ ions at the extreme surface of the electrode. This is confirmed by the lower amount of $Mn^{3+}$ detected by XPS at the surface of the electrode at the end of charge than expected from the electrochemical data (this phenomenon is not observed for $LiFePO_4$). Upon discharge, a partial dissolution of the species deposited at the $LiFe_{0.33}Mn_{0.67}PO_4$ electrode surface occurs. Although good electrochemical performances of $LiFe_xMn_{1-x}PO_4$ electrode materials were shown in previous works [39], the capacity fading of these materials upon long cycling is greater than for $LiFePO_4$. The increased interface reactivity we evidenced in this work certainly impacts the ageing of $LiFe_xMn_{1-x}PO_4$ // graphite cells upon long cycling. Further investigation are in progress to evaluate the influence of this interface reactivity on aging processes of $LiFe_{0.33}Mn_{0.67}PO_4$ // graphite cells.

**Acknowledgments**

The authors thank Süd Chemie Company for providing electrode materials and ANR (National Research Agency) Stock-E program (ANR-09-STOCK-E-07) for financial support, in the frame of the PHOSPHALiON project.

**References**


1. Padhi, A. K.; Nanjundaswamy, K. S.; Goodenough, J. B., *J. Electrochem. Soc.* **1997,** 144, 1188.

2. Padhi, A. K.; Nanjundaswamy, K. S.; Masquelier, C.; Okada, S.; Goodenough, J. B., *J. Electrochem. Soc.* **1997,** 144, 1609.

3. Ravet, N.; Chouinard, Y.; Magnan, J. F.; Besner, S.; Gauthier, M.; Armand, M., *J. Power Sources* **2001,** 97-98, 503.

4. Wang, J.; Liu, P.; Hicks-Gamer, J.; Sherman, E.; Soukiazian, S.; Verbrugge, M.; Tataria, H.; Musser, J.; Finamore, P., *J. Power Sources* **2011,** 196, 3942.

5. Yamada, A.; Chung, S.-C.; Hinokuma, K., *J. Electrochem. Soc.* **2001,** 148, A224.

6. Zhang, P.; Wu, Y.; Xu, Q.; Liu, J.; Ren, X.; Luo, Z.; Wang, M.; Hong, W., *J. Phys. Chem. A* **2008,** 112, 5406.

7. Yamada, A.; Chung, S.-C., *J. Electrochem. Soc.* **2001,** 148, A960.

8. Yonemura, M.; Yamada, A.; Takei, Y.; Sonoyama, N.; Kanno, R., *J. Electrochem. Soc.* **2004,** 151, A1352.

9. Delacourt, C.; Laffont, L.; Bouchet, R.; Wurm, C.; Leriche, J. B.; Morcrette, M.; Tarascon, J.-M.; Masquelier, C., *J. Electrochem. Soc.* **2005,** 152, A1352.

10. Rissouli, K.; Benkhouja, K.; Ramos-Barrado, J. R.; Julien, C., *Mater. Sci. Eng. B* **2003,** 98, 185.

11. Yamada, A.; Kudo, Y.; Liu, K.-Y., *J. Electrochem. Soc.* **2001,** 148, A1153.

12. Meethong, N.; Kao, Y.-H.; Tang, M.; Huang, H.-Y.; Craig Carter, W.; Chiang, Y.-M., *Chem. Mater.* **2008,** 20, 6189.

13. Delacourt, C.; Poizot, P.; Morcrette, M.; Tarascon, J.-M.; Masquelier, C., *Chem. Mater.* **2004,** 16, 93.

14. Martha, S. K.; Markovsky, B.; Grimblat, J.; Gofer, Y.; Haik, O.; Zinigrad, E.; Aurbach, D.; Drezen, T.; Wang, D.; Deghenghi, I.; Exnar, I., *J. Electrochem. Soc.* **2009,** 156, A541.

15. Oh, S.-M.; Oh, S. W.; Yoon, C.-S.; Scrosati, B.; Amine, K.; Sun, Y.-K., *Adv. Funct. Mater.* **2010,** 20, 3260.

16. Wang, D.; Buqa, H.; Crouzet, M.; Deghenghi, I.; Drezen, T.; Exnar, I.; Kwon, N.-H.; Miners, J. H.; Poletto, L.; Graetzel, M., *J. Power Sources* **2009,** 189, 624.

17. Martha, S. K.; Grimblat, J.; Haik, O.; Zinigrad, E.; Drezen, T.; Miners, J. H.; Exnar, I.; Andreas, K.; Markovsky, B.; Aurbach, D., *Angew. Chem. Int. Ed.* **2009,** 48, 8559.

18. Oh, S.-M.; Jung, H.-G.; Yoon, C.-S.; Myung, S.-T.; Chen, Z.; Amine, K.; Sun, Y.-K., *J. Power Sources* **2011,** 196, 6924.

19. Wang, D.; Ouyang, C.; Drezen, T.; Exnar, I.; Kay, A.; Kwon, N.-H.; Gouerec, P.; Miners, J. H.; Wang, M.; Graetzel, M., *J. Electrochem. Soc.* **2010,** 157, A225.

20. Yamada, A.; Kudo, Y.; Liu, K.-Y., *J. Electrochem. Soc.* **2001,** 148, A747.

21. Perea, A.; Castro, L.; Aldon, L.; Stievano, L.; Dedryvere, R.; Gonbeau, D.; Tran, N.; Nuspl, G.; Breger, J.; Tessier, C., *J. Solid State Chem.* **2012,** in press.

22. Shirley, D. A., *Phys. Rev. B* **1972,** 5, 4709.

23. Scofield, J. H., *J. Electron Spectrosc. Relat. Phenom.* **1976,** 8, 129.

24. Castro, L.; Dedryvere, R.; Ledeuil, J.-B.; Breger, J.; Tessier, C.; Gonbeau, D., *J. Electrochem. Soc.* **2012,** 159, A357.

25. Hamelet, S.; Gibot, P.; Casas-Cabanas, M.; Bonnin, D.; Grey, C. P.; Cabana, J.; Leride, J.-B.; Rodriguez-Carvajal, J.; Courty, M.; Levasseur, S.; Carlach, P.; Van Thournout, M.; Tarascon, J.-M.; Masquelier, C., *J. Mater. Chem.* **2009,** 19, 3979.

26. Martin, J.-F.; Cuisinier, M.; Dupre, N.; Yamada, A.; Kanno, R.; Guyomard, D., *J. Power Sources* **2011,** 196, (2155).

27. Palomares, V.; Goni, A.; De Muro, I. G.; Lezama, L.; De Meatza, I.; Bengoechea, M.; Boyano, I.; Rojo, T., *J. Electrochem. Soc.* **2011,** 158, A1042.

28. Fong, R.; Von Sackem, U.; Dahn, J. R., *J. Electrochem. Soc.* **1990,** 137, 2009.

29. Hufner, S., *Photoelectron Spectroscopy: principles and applications*. Springer-Verlag 1995.

30. Dedryvere, R.; Maccario, M.; Croguennec, L.; Le Cras, F.; Delmas, C.; Gonbeau, D., *Chem. Mater.* **2008,** 20, 7164.

31. Van Veenendaal, M. A.; Heskes, H.; Sawatzky, G. A., *Phys. Rev. B* **1993,** 47, 11462.

32. Van Veenendaal, M. A.; Sawatzky, G. A., *Phys. Rev. Lett.* **1993,** 70, 2459.

33. Dedryvere, R.; Foix, D.; Franger, S.; Patoux, S.; Daniel, L.; Gonbeau, D., *J. Phys. Chem. C* **2010,** 114, 10999.

34. Leroy, S.; Blanchard, F.; Dedryvere, R.; Martinez, B.; Carre, D.; Lemordant, D.; Gonbeau, D., *Surf. Interf. Analysis* **2005,** 37, 773.

35. Aurbach, D.; Daroux, M. L.; Faguy, P. W.; Yeager, E., *J. Electrochem. Soc.* **1987,** 134, 1611.

36. Peled, E.; Golodnisky, D., *Lithium-Ion Batteries: Solid Electrolyte Interphase*. 2004.

37. Laruelle, S.; Pilard, S.; Guenot, P.; Grugeon, S.; Tarascon, J.-M., *J. Electrochem. Soc.* **2004,** 151, A1202.

38. Augustsson; Herstedt, M.; Guo, J.-H.; Edstrom, K.; Zhuang, G. V.; Ross, P. N.; Rubensson, J.-E.; Nordgren, J., *Phys. Chem. Chem. Phys.* **2004,** 6, 4185.

39. M. Jo, H. C. Yoo, Y. S. Jung, J. Cho, *J. Power Sources* **2012**, *216*, 162.